Synthesis and characterisation of cyanide bridged heterobinuclear complexes based on Group VI octacyanometalate(IV) and pentaammineosmium(III) ions: a comparison with Group VIII hexacyano analogues

W.M. Laidlaw and R.G. Denning*
Inorganic Chemistry Laboratory, South Parks Road, Oxford OX1 3QR (UK)

(Received December 24, 1993)

Abstract

Two new mixed-valence complexes of the form, $[(NC)_7M'^{IV}(\mu\text{-CN})Os^{III}(NH_3)_5]Li\cdot 2H_2O$ (M′ = Mo, W) have been synthesised and characterised by spectroscopic and electrochemical techniques. The complexes exhibit moderately intense intervalence charge transfer (IVCT) transitions for M′ = Mo at 638 nm ($\epsilon_{max} \approx 1000$ M^{-1} cm^{-1}) and for M′ = W at 717 nm ($\epsilon_{max} \approx 1500$ M^{-1} cm^{-1}). The Hush parameters reveal Robin and Day Class II behaviour ($\alpha^2 < 0.6\%$; $H_{rp} \approx 1000$ cm^{-1}). The IVCT bandwidths are unusually narrow ($\Delta\nu_{1/2} \approx 3400$ M^{-1} cm^{-1}) relative to the well-known Group VIII hexacyano analogues, $[(NC)_5M'^{II}(\mu\text{-CN})Os^{III}(NH_3)_5]^-$ (aq) (M′ = Ru, Os), and are attributed to a combination of reduced Franck–Condon barriers to electron transfer and the exclusion of spin–orbit broadening. Electrochemical measurements reveal an octacyanometalate(IV/V) based irreversible couple at +0.72 V (M′ = Mo) and a near-reversible couple at +0.445 V (M′ = W) in 0.2 M KCl(aq) (versus SCE) for the novel complexes.

Key words: Molybdenum complexes; Tungsten complexes; Osmium complexes; Cyano complexes; Ammine complexes; Mixed-valence complexes

Introduction

Cyanide bridged heterobinuclear complexes based on the Group VIII hexacyanometalate(II) donor and penta- or tetraamminemetal(III) acceptor systems have been studied by several workers [1]. Recently analogues containing polypyridylcyanoruthenium(II) and -osmium(II) donor moieties have been reported [2–4]. The study of such mixed-valence systems has yielded important information about the donor–acceptor coupling through spectroscopic [1, 5] and electrochemical experiments [1], and mode-by-mode assessments of Franck–Condon barriers to electron transfer using resonance Raman spectroscopy [6]. More recently, fundamental aspects of electron transfer dynamics have been investigated using an IR probe of excited state relaxations [7, 8] on the picosecond timescale.

Although octacyano complexes of Group VI metals have been known for many decades and exhibit similar properties [9] to the hexacyano complexes of Group VIII, there appears to have been no attempt to prepare mixed-valence compounds (MVCs) containing these donor systems. Here we report the synthesis of two such complexes, $[(NC)_7M'^{IV}(\mu\text{-CN})Os^{III}(NH_3)_5]Li\cdot 2H_2O$ (M′ = Mo, W) and discuss their spectroscopic and electrochemical characteristics with their hexacyano analogues, $[(NC)_5M'^{II}(\mu\text{-CN})Os^{III}(NH_3)_5]Li\cdot 3H_2O$ (M′ = Ru, Os). Henceforth we unambiguously abbreviate these complexes to **MoOs**, **WOs**, **RuOs** and **OsOs**.

As background, we recall briefly the Hush formulas [10] (eqns. (3)–(5)) and their basis [11]. Let the wavefunctions ψ_r and ψ_p describe the fully localised ground state redox isomer configurations M′(IV)(μ-CN)M(III) and M′(V)(μ-CN)M(II), respectively. Assuming a suitable perturbation matrix element exists to mix the two configurations together, the true ground state, Ψ_G, may be approximated through an LCAO method (eqn. (1)). In the limit of zero-differential overlap ($S_{rp} \rightarrow 0$), eqn. (2) is valid which defines the ground state valence delocalisation coefficient, α (eqn. (5)). The resonance integral H_{rp} reduces to an intermetallic interaction energy in this limit [12]. The Hush formulas are ap-

*Author to whom correspondence should be addressed.

SSDI 0020-1693(94)03843-D

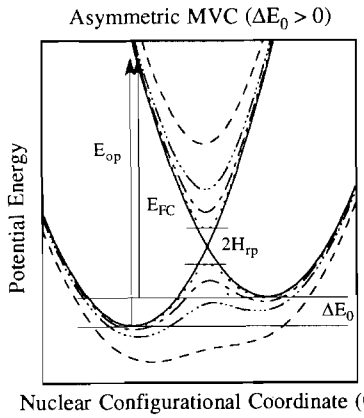

Fig. 1. Schematic configuration–energy diagram for an asymmetric mixed-valence complex showing the effect of coupling between the redox isomers and defining various parameters.

plicable to MVCs in which $\alpha^2 \ll 1$, corresponding to the weak coupling limit described, in the Robin and Day scheme [13], as Class II. The coupling parameters, α and H_{rp}, can be derived from the energy (ν_{max}), bandwidth ($\Delta\nu_{1/2}$) and extinction coefficient (ϵ_{max}) of the optical intervalence charge transfer (IVCT) transition. The intermetallic distance, d, is in Ångstroms.

$$\Psi_G = a\psi_r + b\psi_p \quad \text{for } a^2 + b^2 \pm 2abS_{rp} = 1 \tag{1}$$

$$\Psi_G = (1-\alpha^2)^{1/2}\psi_r + \alpha\psi_p \tag{2}$$

$$\Delta\nu_{1/2}(\text{cm}^{-1}) = \sqrt{16(\log_e 2)kT(E_{op} - \Delta E_0)} = \sqrt{2310(E_{op} - \Delta E_0)} \tag{3}$$

$$H_{rp}(\text{cm}^{-1}) = \nu_{max}\alpha = 2.05 \times 10^{-2}\left(\frac{\nu_{max}}{d}\right)\sqrt{\frac{\epsilon_{max}\Delta\nu_{1/2}}{\nu_{max}}} \tag{4}$$

$$\alpha^2 = 4.24 \times 10^{-4}\left(\frac{\epsilon_{max}\Delta\nu_{1/2}}{\nu_{max}d^2}\right) \tag{5}$$

$$E_{op} = E_{FC} + \Delta E_0 = \chi_i + \chi_o + \Delta E_0 \tag{6}$$

In terms of potential energy surfaces, Fig. 1 presents the coupling scenario and relates the relevant electronic parameters discussed later. The solid lines refer to the strictly localised wavefunctions ψ_r and ψ_p and the broken lines to the eigenstates allowing varying degrees of electronic coupling. The degree of electronic asymmetry is denoted by ΔE_0. The IVCT is denoted by E_{op} and has constituent inner- (χ_i) and outer-sphere (χ_o) contributions to the Franck–Condon barrier E_{FC}.

Experimental

Syntheses

The complexes, $K_4Mo(CN)_8 \cdot 2H_2O$, $K_4W(CN)_8 \cdot 2H_2O$ and $[Os(NH_3)_5(OSO_2CF_3)](CF_3SO_3)_2$ were prepared by literature methods [14, 15]. The mixed-valence species, $[(NC)_5M'^{II}(\mu\text{-}CN)Os^{III}(NH_3)_5]^-$ M' = Ru, Os) were prepared following Vogler *et al.* [5] but, without modification to the purification procedures, analytically pure products could not be obtained. Pure samples could be isolated, however, as lithium trihydrates using Sephadex DEAE A-25; 40–120 μm mesh anion exchange columns with 0.075–0.2 M LiCl(aq) eluting solutions. Crystalline products were isolated by evaporation and precipitation as described below.

$[(NC)_7M'^{IV}(\mu\text{-}CN)Os^{III}(NH_3)_5]Li \cdot 2H_2O$

NB. As far as possible all manipulations involving solutions of octacyano derivatives should be conducted in the dark.

(a) M' = Mo. A sample of $K_4Mo(CN)_8 \cdot 2H_2O$ (0.5 g, 1.0 mmol) is dissolved in water (15 ml) which is then purged with nitrogen. Two drops of trifluoroacetic acid are added. Small portions of powdered $[Os(NH_3)_5(OSO_2CF_3)](CF_3SO_3)_2$ (0.6 g, 0.83 mmol) are added over 1 h such that the next portion is added after the previous one has completely dissolved. The solution is left to react for a further 7 h. The turquoise (green for M' = W) solution is passed through a cation exchange column (Dowex 50W-X8(Na^+); 18–52 mesh; 1×12 cm). The column is washed with a little water and the combined solutions adsorbed onto an anion exchange column (Sephadex DEAE A-25; 40–120 μm mesh; 1×12 cm) which is then washed with water. The product is best eluted from the Sephadex column using 0.5 M LiCl(aq). Unreacted yellow octacyano species remain on the column. The product is isolated by reducing the volume of the eluted solution (10 ml), adding excess methanol and sufficient acetone to induce precipitation followed by refrigeration. The turquoise (green for M' = W) solid was filtered off, washed with methanol, acetone and diethyl ether and vacuum dried immediately. The product is hygroscopic. Yield 30%. *Anal.* Calc. for $C_8H_{19}LiMoN_{13}O_2Os$ (M_r = 622.4): C, 15.4; H, 3.1; N, 29.3. Found: C, 15.4; H, 3.1; N, 27.5%.

(b) M' = W. Method (a) is followed using $K_4W(CN)_8 \cdot 2H_2O$ (0.6 g, 1.0 mmol) and $[Os(NH_3)_5(OSO_2CF_3)](CF_3SO_3)_2$ (0.6 g, 0.83 mmol). *Anal.* Calc. for $C_8H_{19}LiN_{13}O_2OsW$ (M_r = 710.4): C, 13.5; H, 2.7; N, 25.6. Found: C, 13.1; H, 2.7; N, 23.7%.

Instrumentation

IR spectra were recorded with 2 cm^{-1} resolution on a Mattson Polaris FTIR instrument in KBr pellets. Absorption spectra were obtained using a Perkin-Elmer Lambda 9 spectrometer with computer interface. The cyclic voltammetric measurements were performed on a Princeton Applied Research potentiostat (model 273) with a conventional three-armed cell using a standard saturated KCl calomel reference electrode with Pt bead working and Pt wire counter electrodes in 0.2 M KCl(aq) electrolytic media for all the octacyano complexes. The potentials for the hexacyano species (Table 2), available from previous work, were recorded using a glassy carbon working electrode and Pt mesh counter electrode under otherwise identical conditions. Cycles were recorded at scan rates of 100, 200 and 400 mV s^{-1}, from low–high–low potential, with typical peak wave currents of the order 50 μA. Microanalyses were made by the departmental facility.

Results and discussion

Infrared spectra

Figure 2 and Table 1 show the IR data for the molybdenum(IV) and tungsten(IV) octacyano precursors and their associated pentaammineosmium(III) MVCs in the window 2000–2200 cm^{-1}.

The symmetry of the octacyanometalates has been discussed at length in the literature [9]; the results favour a dodecahedral (D_{2d}) rather than a square-antiprismatic (D_{4d}) structure for the potassium salts [16]. Assigning the IR spectral bands in the cyanide region of the spectra (Fig. 2) is well documented [17] for the octacyano precursors (bracketed labels in Table 1) but is non-trivial for the MVCs. The bands almost certainly consist of unresolved overlapping absorptions on account of the very low symmetry. By analogy with the spectrum of $[(NC)_5Ru^{II}(\mu\text{-}CN)Ru^{III}(NH_3)_5]^-$ one expects the bridging cyanide to be at a higher frequency than in the mononuclear precursor [6]. The IR features of the octacyano MVCs resemble each other very closely although the molybdate bands appear to have shifted more than those of the tungstate upon metalation.

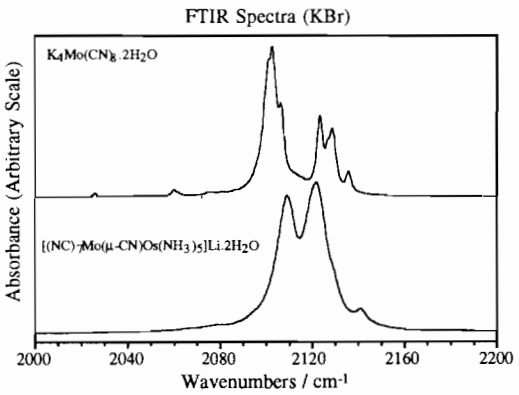

Fig. 2. Polycrystalline pellet (KBr) IR spectra, in the cyanide window, for the octacyanomolybdate (upper) and its associated mixed-valence complex (lower).

TABLE 1. Polycrystalline pellet (KBr) IR data, in the cyanide window, for the octacyanometalate and associated mixed-valence complexes

Complex	IR[a] (KBr) (cm^{-1})
$K_4[Mo(CN)_8]\cdot 2H_2O$	2060vw(i), 2103vs(e), 2106sh(b_2), 2124m(b_2), 2129m(e), 2136w(a_1)
$K_4[W(CN)_8]\cdot 2H_2O$	2055vw(i), 2096vs(e), 2101sh(b_2), 2124m(b_2), 2130m(e), 2138w(a_1)
MoOs	2109vs, 2122vs, 2141w
WOs	2095vs, 2119vs, 2142w

[a]Abbreviations: v = very, s = strong, m = medium, w = weak, sh = shoulder. Labels refer to mode assignments based on D_{2d} symmetry; (i) = isotope peak. The a_1 mode is only Raman active but is weakly observed due to site symmetry effects.

TABLE 2. Electrochemical data for the octacyanometalate and associated mixed-valence complexes

Complex	$E_{p,a}$ (V)	$E_{p,c}$ (V)	$E_{1/2}$ (V)
$K_4Ru(CN)_6\cdot 3H_2O$	+0.85	+0.655	+0.75
$K_4Os(CN)_6\cdot 3H_2O$	+0.615	+0.275	+0.445
$K_4Mo(CN)_8\cdot 2H_2O$	+0.60	+0.52	+0.56
$K_4W(CN)_8\cdot 2H_2O$	+0.345	+0.25	+0.30
MoOs	+0.775	+0.66	+0.72
WOs	+0.49	+0.40	+0.445

$E_{p,a}$ and $E_{p,c}$ are the peak anodic (oxidative) and cathodic (reductive) potentials and $E_{1/2} = 1/2(E_{p,a} + E_{p,c})$. Values quoted for 100 mV s^{-1} except for **MoOs** at 400 mV s^{-1}.

Electrochemistry

Cyclic voltammetric data is shown in Table 2 and Fig. 3 for both MVCs (solid traces) and also for the mononuclear octacyano precursors (dashed traces). The redox waves correspond to octacyanometalate(IV/V) processes.

In each case binuclear complex formation increases the redox potential of the cyanometalate centre, by $\approx$0.15 V, primarily through ion charge rather than coupling effects. The half-wave peak potential separations are all greater than the predicted 59 mV for reversible reactions and increase slightly with scan rate. The peak current ratios indicate reversible ($i_{p,a}/i_{p,c} = 1$) and diffusion controlled ($i_p/\nu^{1/2}$ = constant; ν is the scan rate) behaviour for the precursor octacyanometalates but show varying deviations for the dimers. The octa-

TABLE 3. Intervalence charge transfer characteristics of the Group VI octacyano- and Group VIII hexacyano-pentaammineosmium(III) mixed-valence complexes

MVC[a]	E_{op} (nm)	E_{op} (cm^{-1})	ϵ_{max} (M^{-1} cm^{-1})	$\Delta\nu_{1/2}$ (cm^{-1})	α^2 (%)	H_{rp} (cm^{-1})	f
RuOs	491	20360	2460	4460	0.84	1865	0.0505
OsOs	556	17980	2540	7075	1.57	2255	0.0827
MoOs	638	15670	995	3430	0.34	915	0.0157
WOs	717	13945	1460	3340	0.55	1030	0.0224

[a]Mixed-valence complexes of the form, $[(NC)_5M'^{II}(\mu\text{-}CN)Os^{III}(NH_3)_5]Li\cdot 3H_2O$ (M′ = Ru, Os) and $[(NC)_7M'^{IV}(\mu\text{-}CN)Os^{III}(NH_3)_5]Li\cdot 2H_2O$ (M′ = Mo, W). Oscillator strengths, f, are calculated assuming gaussian envelopes from $f \approx 4.6\times10^{-9}\ \epsilon_{max}\ \Delta\nu_{1/2}$. Coupling parameters are calculated from eqns. (4) and (5) using an intermetallic separation of 5.2 Å.

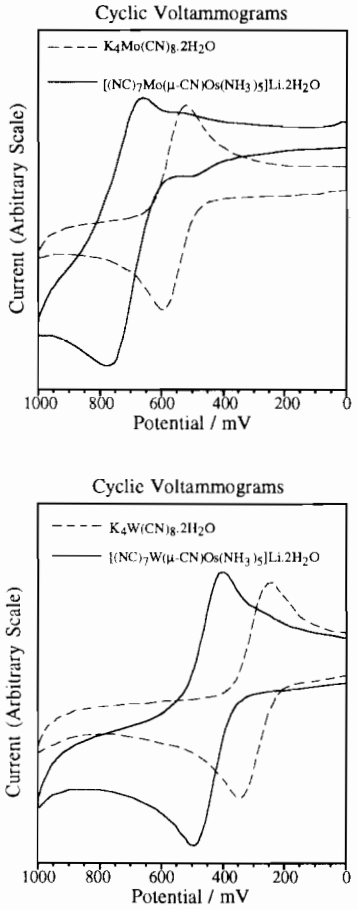

Fig. 3. Cyclic voltammograms of the octacyanometalates (– – –) and their associated mixed-valence complexes (——).

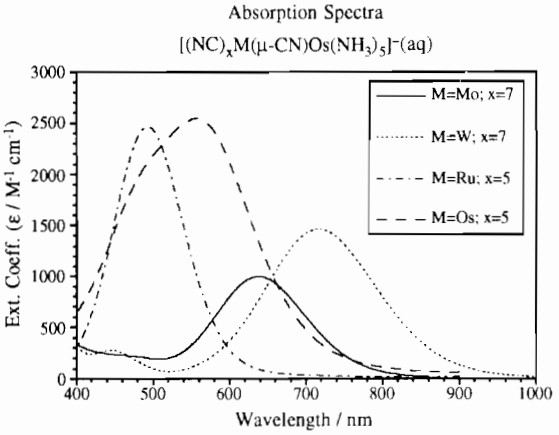

Fig. 4. Electronic absorption spectra showing the intervalence charge transfer bands of the Group VI octacyano- and Group VIII hexacyano-pentaammineosmium(III) mixed-valence complexes.

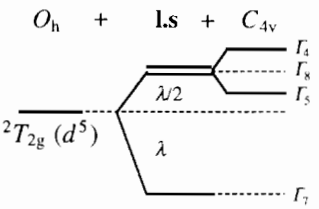

Fig. 5. Schematic diagram showing the effect of strong spin–orbit coupling and weak tetragonal field upon the octahedral term $^2T_{2g}$ (d^5).

cyanomolybdate centre in **MoOs** is clearly irreversible whereas reversibility ($i_{p,a}/i_{p,c} = 1.0$) is retained in **WOs**.

Absorption spectra

Aqueous solutions of the Group VI MVCs slowly decrease in intensity and become cloudy on prolonged exposure to sunlight and were therefore always handled in the dark. Table 3 details the electronic absorption characteristics of the IVCT process together with the calculated Hush parameters (eqns. (3)–(5)). Figure 4 shows the associated absorption profiles for all four MVCs. All the MVCs are Class II systems exemplified by the small mixing functions α^2 and H_{rp}.

The IVCT bandwidth of **OsOs** is notably much broader ($\Delta\nu_{1/2} \approx 7000\ cm^{-1}$) than the other complexes and exhibits a pronounced high energy asymmetry. We attribute these effects to spin–orbit splitting in the hexacyanoosmate(III) (d^5) excited states rather than in the pentaamminemetal(III) (d^5) ground state (Fig. 5). The IVCT band of **RuOs** ($\Delta\nu_{1/2} \approx 4500\ cm^{-1}$) does not reveal this asymmetry because the spin–orbit coupling parameter is much smaller than the bandwidth, $\zeta(Ru^{III}) \approx 1250\ cm^{-1}$ and $\zeta(Os^{III}) \approx 3000\ cm^{-1}$ [18], although the high

energy side of the band has a larger half-bandwidth than the low energy side. By analogy one might expect a similarly large spin–orbit broadening in **WOs** compared to **MoOs** since $\zeta(Mo^V) \approx 900$ cm^{-1} and $\zeta(W^V) \approx 2700$ cm^{-1} [18]. This is not observed; both MVCs have narrow bandwidths ($\Delta\nu_{1/2} \approx 3400$ cm^{-1}). The lack of spin–orbit asymmetry is readily understood in terms of the absence of orbital degeneracy of the d^1 configuration in the D_{2d} environment. Butler *et al.* [19] report the appropriate energy level diagram for $[M^V(CN)_8]^{3-}$ the important characteristics of which are a non-degenerate ground state separated from degenerate excited states by more than 20 000 cm^{-1}.

Vogler *et al.* [5] have shown that differences in IVCT energies (ΔE_{op}) between hexacyanometalate MVCs, for a given pentaamminemetal system, correlate well with differences in the redox potentials of the corresponding hexacyanometalate mononuclear precursors ($\Delta E_{1/2}$). For example, between **RuOs** and **OsOs** (Table 3), $\Delta E_{op} \approx 2400$ cm^{-1} and $\Delta E_{1/2} \approx 0.31$ V ($\equiv 2480$ cm^{-1}). That is to say, altering the identity of the metal hexacyanide simply changes the degree of redox asymmetry (ΔE_0) in the MVC corresponding to a relative vertical displacement alone in the potential energy surfaces in Fig. 1. In other words, the Franck–Condon barriers to electron transfer, E_{FC}, are invariant (eqn. (6)). On this basis using the redox potentials of the hexacyanoruthenate(II) and octacyanomolybdate(IV) precursors one would therefore predict the IVCT for **MoOs** to be approximately 1530 cm^{-1} ($\Delta E_{1/2} = 0.19$ V) lower in energy than **RuOs**; that is, the IVCT would be around 532 nm. Table 3 shows that this prediction is very poor. A similar discrepancy exists comparing **OsOs** and **WOs** (Table 3). The lower than expected IVCT energy for the Group VI dimers therefore implies a reduction in the Franck–Condon barrier as well as a change in asymmetry; that is, a relative horizontal potential curve shift as well as a vertical shift, relative to the Group VIII analogues. Assuming outer-sphere contributions (χ_o) to the Franck–Condon energy for the cyanometalates are small and approximately constant, inner-sphere contributions (χ_i) will dominate the differences in E_{FC} (eqn. (6)).

The origin of χ_i lies in oxidation state dependent metal–ligand bond lengths (and angles). These can be determined through appropriate X-ray studies and are reflected in the rate constants of outer-sphere charge transfer processes between redox isomer ion-pairs. The rate constants for the octacyanomolybdate and -tungstate species [20] are at least an order of magnitude greater than for the Group VIII hexacyanometalates indicating a smaller Franck–Condon factor for the former. Limited X-ray data [9, 16] confirm very small metal–ligand bond length variations with oxidation state for the octacyanides. This is consistent with the occupation of a single weakly bonding d orbital in both the d^1 and d^2 species.

In summary therefore, the particularly narrow octacyano dimer IVCT bandwidths are due to absence of a spin–orbit broadening mechanism in D_{2d} symmetry and relatively small inner-sphere contributions to the Franck–Condon barrier.

The metal cyanide IR frequencies are also consistent with this interpretation. In general, t_{2g} electrons will have little effect on metal–cyanide bond strengths, and therefore bond lengths, unless π bonding is important. The stretching frequency of free cyanide [21] occurs at 2078 cm^{-1}. In the Group VIII (Ru, Os) d^6 hexacyanides metal–cyanide π backbonding lowers this frequency (ν(CN) = 2030–2070 cm^{-1}) [21]. On the other hand, the Group VI (Mo, W) d^2 octacyanides (ν(CN) = 2090–2140 cm^{-1}) do not. Instead ν(CN) is dominated by the withdrawal of antibonding σ electrons into the metal–carbon bond.

The lack of significant π backbonding in the Group VI d^2 complexes is also consistent with the relatively small electronic coupling parameters, α^2 and H_{rp}, evident in the much weaker IVCT absorptions. Since direct metal–metal orbital overlap is expected to be minimal over a cyanide bridge (intermetallic separation is ≈ 520 pm) electron transfer predominantly occurs through bridge mediated, π-conjugated superexchange pathways [22, 23]; that is, through donor metal-to-bridge, HOMO–LUMO, overlap and bridge-to-acceptor metal, HOMO–LUMO, overlap. Poor overlap between octacyano metal πd orbitals and the π^* orbitals of the bridging cyanide severely inhibits such mediated pathways.

Acknowledgements

We thank the S.E.R.C. for financial support (W.M.L.), Dr P.D. Beer for the use of electrochemical apparatus and the Clarendon laboratory for electronic absorption facilities.

References

1 Y. Dong and J.T. Hupp, *Inorg. Chem., 31* (1992) 3170, and refs. therein.
2 C.A. Bignozzi, S. Roffia and F. Scandola, *J. Am. Chem. Soc., 107* (1985) 1644.
3 C.A. Bignozzi, C. Paradisi, S. Roffia and F. Scandola, *Inorg. Chem., 27* (1988) 408.
4 J.R. Schoonover, C.J. Timpson, T.J. Meyer and C.A. Bignozzi, *Inorg. Chem., 31* (1992) 3185.
5 A. Vogler, A.H. Osman and H. Kukely, *Inorg. Chem., 26* (1987) 2337.
6 S.K. Doorn and J.T. Hupp, *J. Am. Chem. Soc., 111* (1989) 1142.

7 S.K. Doorn, P.O. Stoutland, R.B. Dyer and W.H. Woodruff, *J. Am. Chem. Soc., 114* (1992) 3133.
8 S.K. Doorn, R.B. Dyer, P.O. Stoutland and W.H. Woodruff, *J. Am. Chem. Soc., 115* (1993) 6398.
9 A.G. Sharpe, *The Chemistry of Cyano Complexes of the Transition Metals,* Academic Press, London, 1976.
10 C. Creutz, *Prog. Inorg. Chem., 28* (1983) 1.
11 R.D. Cannon, *Electron Transfer Reactions,* Butterworths, Guildford, UK, 1980.
12 B. Mayoh and P. Day, *J. Chem. Soc., Dalton Trans.,* (1974) 846.
13 M.B. Robin and P. Day, *Adv. Inorg. Radiochem., 10* (1967) 247.
14 J.G. Leipoldt, L.D.C. Bok and P.J. Cilliers, *Z. Anorg. Allg. Chem., 407* (1974) 350; *409* (1974) 343.
15 P.A. Lay, R.H. Magnusson and H. Taube, *Inorg. Chem., 28* (1989) 3001.
16 A. Samotus and J. Sklarzewicz, *Coord. Chem. Rev., 125* (1993) 63.
17 K.O. Hartmann and F.A. Miller, *Spectrochim. Acta, Part A, 24* (1968) 669.
18 B.N. Figgis, *Introduction to Ligand Fields,* Wiley, New York, 1966.
19 K.R. Butler, T.J. Kemp, B. Sieklucka and A. Samotus, *J. Chem. Soc., Dalton Trans.,* (1986) 1217.
20 F.A. Cotton and G. Wilkinson, *Advanced Inorganic Chemistry,* Wiley, New York, 5th edn., 1988, p. 1308.
21 K. Nakamoto, *Infrared Spectra of Inorganic and Coordination Compounds,* Wiley, New York, 1970.
22 F. Scandola, R. Argazzi, C.A. Bignozzi, C. Chiorboli, M.T. Indelli and M.A. Rampi, *Coord. Chem. Rev., 125* (1993) 283.
23 J.T. Hupp, *J. Am. Chem. Soc., 112* (1990) 1563.